Editors' Suggestion

Soft-mode enhanced type-I superconductivity in $LiPd_2Ge$

Karolina Górnicka,[1,*] Gabriel Kuderowicz,[2] Elizabeth M. Carnicom,[3] Kamil Kutorasiński,[2] Bartlomiej Wiendlocha,[2] Robert J. Cava,[3] and Tomasz Klimczuk[1,†]

[1]*Faculty of Applied Physics and Mathematics and Advanced Materials Centre, Gdansk University of Technology, Narutowicza 11/12, 80-233 Gdańsk, Poland*

[2]*Faculty of Physics and Applied Computer Science, AGH University of Science and Technology, Aleja Mickiewicza 30, 30-059 Kraków, Poland*

[3]*Department of Chemistry, Princeton University, Princeton, New Jersey 08544, USA*

(Received 20 April 2020; revised 11 June 2020; accepted 16 June 2020; published 6 July 2020)

The synthesis, crystal structure, and physical properties (magnetization, resistivity, heat capacity) in combination with theoretical calculations of the electronic structure and phonon properties are reported for intermetallic compounds $LiPd_2X$ (X = Si, Ge, and Sn). LeBail refinement of powder x-ray diffraction data confirms that all compounds belong to the Heusler family (space group Fm-3m, No. 225). The lattice parameter increases with atomic size of X, and its value varies from $a = 5.9059(4)$ Å for $LiPd_2Si$ and $a = 6.0082(3)$ Å for $LiPd_2Ge$, to $a = 6.2644(1)$ Å for $LiPd_2Sn$. The first compound, $LiPd_2Si$, has apparently not been previously reported. All measured quantities demonstrate that $LiPd_2Ge$ exhibits superconductivity below $T_c = 1.96$ K and the normal- and superconducting-state data indicate that it is a weak-strength type-I superconductor ($C/\gamma T_c = 1.38$) with electron-phonon coupling constant $\lambda_{e-p} = (0.53 - 0.56)$. $LiPd_2Si$ and $LiPd_2Sn$ are not superconducting above 1.68 K. The experimental observations are supported by theoretical calculations which show that $LiPd_2Ge$ has the highest computed λ_{e-p} and T_c of the group. A strong softening of the acoustic phonon mode is calculated, and in the case of X = Ge and Sn, imaginary phonon frequencies were computed. The soft mode is most pronounced in the case of $LiPd_2Ge$, which suggests its correlation with superconductivity.

DOI: 10.1103/PhysRevB.102.024507

I. INTRODUCTION

Although discovered more than 100 years ago, the Heusler material classes remain an exciting and active research area. The prototype compound, $MnCu_2Al$, is a ferromagnet at room temperature though it consists of three nonmagnetic metals [1]. Nowadays, there are more than 1000 reported compounds in this family, and they reveal all kinds of physical properties: heavy fermion, shape-memory effect, thermoelectric, and ferromagnetism including half-metallic ferromagnetism. Recently a quantum critical point (QCP) and a new type of interaction between charge density wave (CDW) and superconductivity was found in $Lu(Pt_{1-x}Pd_x)_2In$ [2]. Intriguing physics has been observed in the half-Heusler compounds, e.g., band inversion [3,4] and the coexistence of magnetic ordering and superconductivity [5,6].

The Heusler and half-Heusler ternary intermetallic compounds have the chemical formula AT_2M and ATM, respectively. In the formula, A stands for rare-earth metal but it can also be Li, Be, Mg, and metals from group IV, V, and VI. T is a transition metal from group IX-XI and also Mn, Fe, Ru, Zn, and Cd, while M is an sp metal or metalloid (Sb, Bi). The compounds form in a cubic crystal structure, with the space group Fm-3m (s.g. 225) for the Heusler and F-43m (s.g. 216) for the half-Heusler system. An excellent description with a comparison of the crystal structures of both families, as well as a discussion concerning the chemical nomenclature can be found in Ref. [7].

Superconductivity in this family is rather uncommon. There are only about 30 reported Heusler superconductors. Their physical properties can be tentatively predicted by counting the number of valence electrons (N_{el}). For example, semiconducting behavior is expected for $N_{el} = 18$, whereas superconductivity is expected for $N_{el} = 27$ [7,8]. Interestingly, the number of valence electrons per atom $N_{el}/4 = 6.75$ electrons per atom is close to the second maximum of T_c versus the electron count observed for transition metals [9], and slightly higher than the maximum of T_c at 6.4 electrons per atom observed for $A_{0.25}B_{0.75}$ compounds with the A15 crystal structure [10].

Recently we described a Li-based Heusler superconductor, $LiGa_2Rh$ [11]. This compound is a Bardeen-Cooper-Schrieffer (BCS) superconductor with four valence electrons per atom, which is at the onset of the first superconducting dome proposed for superconducting metals [9,12] and compounds with the A15 crystal structure [10]. Motivated by finding the Li-based Heusler superconductor, we synthesized and tested several $LiPd_2X$ materials (X = Si, Ge, and Sn). In this paper we report type-I superconductivity in $LiPd_2Ge$. According to our knowledge, type-I superconductivity among Heuslers compounds has not been observed.

II. EXPERIMENTAL AND THEORETICAL DETAILS

Polycrystalline samples of $LiPd_2X$ were synthesized by a two-step solid-state reaction. The starting elements were

*karolina.gornicka@pg.edu.pl
†tomasz.klimczuk@pg.edu.pl

high-purity Li chunks (4N, Alfa Aesar), Pd powder (4N8, Mennica-Metale, Poland), Ge powder (4N, Alfa Aesar), Si pieces (3N, Alfa Aesar), and Sn pellets (4N, Alfa Aesar). An excess of lithium (10%) was added in order to compensate for the loss during synthesis. The following manipulations were performed in a protective Ar atmosphere in a glove box system [$p(O_2) < 0.5$ ppm]. All materials were mixed together, pressed into a pellet using a hydraulic press, placed in a tantalum crucible, and then sealed inside an Ar-filled quartz tube. The ampoule was slowly heated to 240 °C at a rate of 2.5 °C/h and then heated to 550 °C (10 °C/h), held at that temperature for 12 h, and air quenched to room temperature. The as-prepared material was reground well and once more pressed into a pellet. The samples were then enclosed inside a quartz tube and annealed at 610 °C for 3 days. No melting was observed and the resulting materials were dense and brown in color.

The chemical composition and phase purity of $LiPd_2Ge$ were measured using an FEI Quanta 250 FEG scanning electron microscope (SEM) equipped with an Apollo-X SDD energy-dispersive spectrometer (EDS). The data were analyzed using EDAX TEAM^{tm} software. Room-temperature powder x-ray diffraction (pXRD) characterization was carried out on a Bruker D2 phaser diffractometer with Cu $K\alpha$ radiation ($\lambda = 1.5406$ Å) and a LynxEye-XE detector. The data were collected from $10^\circ - 90^\circ$ 2θ over 120 minutes of scan time. LeBail refinement of the pXRD pattern was performed to determine the lattice parameters, using the DIFFRAC.SUITE TOPAS. Temperature- and field-dependent magnetization measurements were performed in a Quantum Design Dynacool Physical Property Measurement System (PPMS) with a vibrating sample magnetometer (VSM) function. The data were collected in the temperature range of 1.68–2.1 K under various applied magnetic fields. The heat capacity was measured using the two-τ time-relaxation method in a PPMS Evercool II system in the temperature range 1.81–300 K. The sample was attached to the measuring stage using Apiezon N grease to ensure good thermal contact. The electrical resistivity measurements were performed by a conventional four-probe method using the ac transport option of the PPMS Evercool II system from 1.81 to 300 K. The electrical leads were small-diameter Pt wires attached to the polished sample using conductive silver epoxy (Epotek H20E).

Electronic structure, phonons, and the electron-phonon interaction functions were calculated using density functional theory with the plane-wave pseudopotential method as implemented in the QUANTUM ESPRESSO (QE) package [13,14]. We used the projector augmented wave pseudopotentials [15,16] and the Perdew-Burke-Ernzerhof generalized gradient approximation exchange-correlation functional [17]. Energy cutoffs for wave functions and charge densities were set to 60 and 600 Ry, respectively. A 24^3 k-point Monkhorst-Pack grid for the electronic structure and 8^3 q-point grid for the interatomic force constant calculations were employed. Both scalar-relativistic and full-relativistic [including spin-orbit coupling (SOC)] calculations of the electronic structure were done.

Firstly, $LiPd_2X$ (X = Si, Ge, Sn) unit cells were relaxed with the Broyden-Fletcher-Goldfarb-Shanno algorithm. The experimental lattice constants and the calculated ones are shown in Table I. The calculated lattice constants are slightly larger than the experimental ones, which is usually the case when using GGA functionals. The atomic positions are fixed by the symmetry, and therefore they were not changed in the relaxation. The volume relaxation was repeated with SOC included, but no important difference was found. For the relaxed structures, the electronic dispersion relations, densities of states (DOS), and Fermi surface were calculated. Using density functional perturbation theory [18], phonons and electron-phonon interaction functions (Eliashberg functions) were computed. As SOC was found to have a negligible effect on the electronic structure, phonon and electron-phonon calculations were done in a scalar-relativistic way, with an additional test of phonon frequencies calculated with SOC for a selected **q**-vector for $LiPd_2Ge$.

TABLE I. Experimental and calculated lattice constant a for the $LiPd_2X$ family.

	$LiPd_2Si$	$LiPd_2Ge$	$LiPd_2Sn$
Experimental (Å)	5.9059(4)	6.0082(3)	6.2644(1)
Calculated w/o SOC (Å)	5.9512	6.0780	6.3367
Calculated with SOC (Å)	5.9518	6.0799	6.3370

III. RESULTS OF THE EXPERIMENTAL STUDIES

The sample of $LiPd_2Ge$ was first examined using an energy dispersive spectrometer (EDS). High-resolution SEM images showed that the sample is uniform and the EDS analysis within experimental error confirmed Pd:Ge ratio near expected 2:1, consistent with the nominal composition.

The LeBail refinement of the powder x-ray diffraction pattern (Fig. S1 in the Supplemental Material (SM) [19]) for $LiPd_2Si$, $LiPd_2Ge$, and $LiPd_2Sn$ confirms that all compounds crystallize in the cubic $L2_1$ crystal structure (space group Fm-$3m$, No. 225). Lattice parameters obtained from the refinements are $a = 5.9059(4)$ Å for $LiPd_2Si$, $a = 6.0082(3)$ Å for $LiPd_2Ge$, and $a = 6.2644(1)$ Å for $LiPd_2Sn$. We have not seen reports of $LiPd_2Si$, and the cell parameter values for the other two compounds are in very good agreement with previously published data [20]. The pXRD analysis confirms the good quality of the examined samples. The difference plot (between experimental and fitted data) and the Bragg positions is also shown in Fig. S1 [19]. Additional pXRD scans were performed on a pulverized sample exposed to air for 12 h. The obtained patterns confirm stability of all compounds over that time period.

The temperature-dependent volume magnetic susceptibility, defined as $\chi = dM/dH$ where M is the magnetization and H is the applied magnetic field, for $LiPd_2Ge$ is shown in Fig. 1(a). Both zero-field-cooled (ZFC) and field-cooled (FC) data show a sharp diamagnetic transition, corresponding to the onset of superconductivity. The critical temperature, $T_c = 1.96$ K, was determined as the intersection between a line drawn at the steepest slope of the superconducting signal and the extrapolation of the normal-state magnetic susceptibility [21]. After considering the demagnetization effect of the sample by using the formula $-4\pi\chi_V = 1/(1-N)$, where

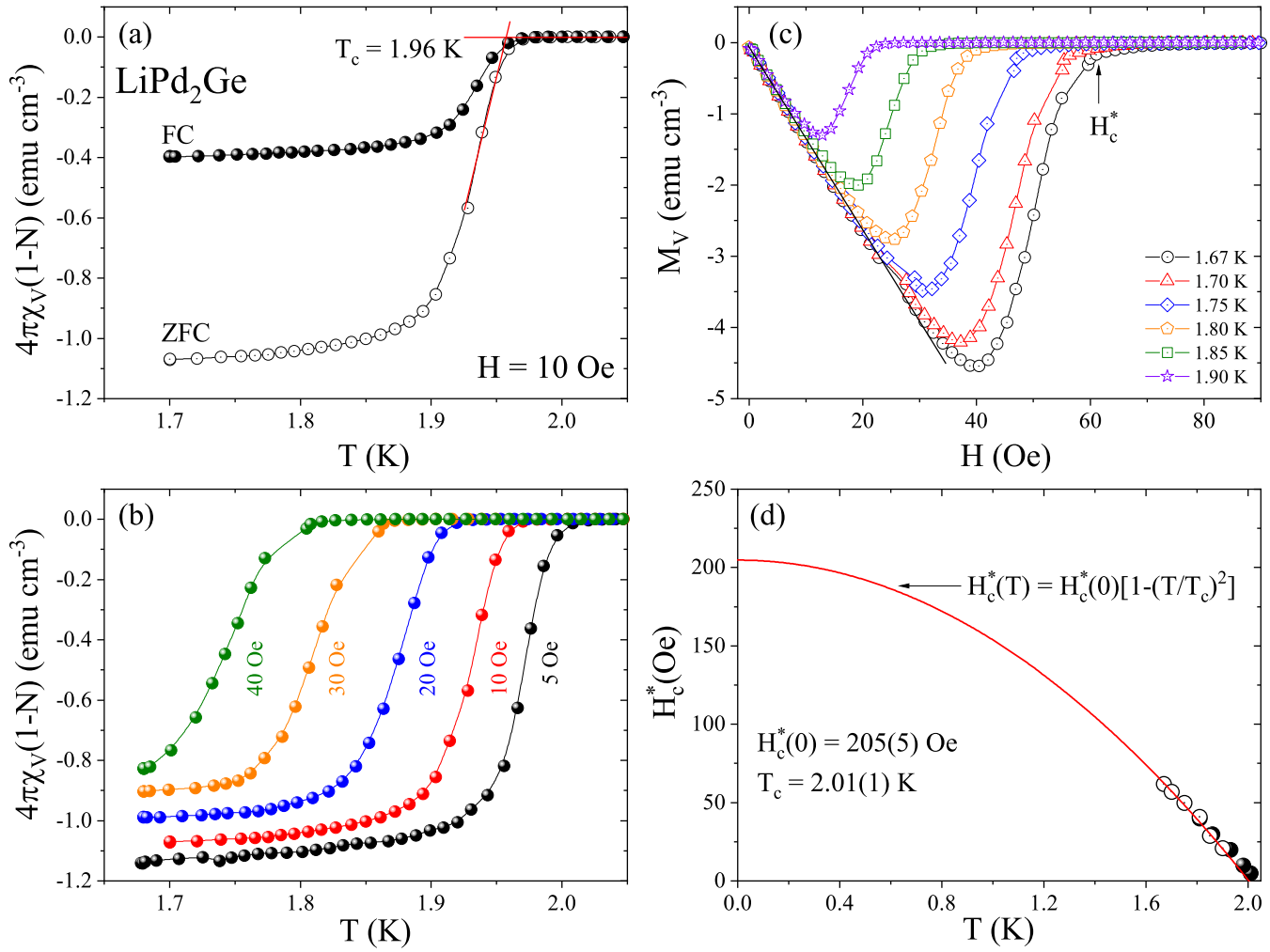

FIG. 1. Magnetic characterization of the superconductivity of $LiPd_2Ge$. (a) Zero-field-cooled (open circles) and field-cooled (full circles) temperature-dependent magnetic susceptibility data in $H = 10$ Oe. (b) The temperature-dependent magnetic susceptibility data for $5\,\text{Oe} \leqslant H \leqslant 40\,\text{Oe}$. (c) Field-dependent magnetization data at various temperatures. (d) Thermodynamic critical field $H_c^*(0)$ determined from $\chi_v(T)$ (full circles) and $M_V(H)$ (open circles).

$N = 0.4$ is the geometrical demagnetization factor [estimated from the $M_V(H)$ fit discussed later], the ZFC data are consistent with a 100% Meissner volume fraction, indicating bulk superconductivity in $LiPd_2Ge$. The FC diamagnetic signal at the lowest temperature is relatively strong, which might suggest that the grains are large and hence not much magnetic field is trapped at the grain boundaries. Figure 1(b) presents the ZFC data at various externally applied magnetic fields ($5\,\text{Oe} \leqslant H \leqslant 40\,\text{Oe}$). The application of the magnetic field suppressed the critical temperature gradually. This allows us to extract the values of the critical field H_c, represented with full circles in Fig. 1(d). The volume magnetization isotherms $M_V(H)$, taken at different temperatures below T_c, are shown in Fig. 1(c). Assuming that the initial response to a magnetic field is perfectly diamagnetic, we obtained a demagnetization factor $N = 0.4$. It is clear that the plotted curves of $M_V(H)$ show a steplike jump to zero near the critical field, indicating type-I superconductivity in $LiPd_2Ge$. The critical field value, H_c^*, was determined as the entrance to the normal state, at each temperature. The variation of H_c^* with temperature is depicted in Fig. 1(d), where full circles are obtained from the $\chi_v(T)$ analysis and open circles are data points taken from the $M_V(H)$ measurements. The solid red line gives the fit that uses temperature dependence:

$$H_c^*(T) = H_c^*(0)\left[1 - \left(\frac{T}{T_c}\right)^2\right], \tag{1}$$

where $H_c^*(0)$ is the critical field at 0 K and T_c is the superconducting critical temperature. The experimental data are well described with the above formula and a fit gives $H_c^*(0) = 205(5)$ Oe and $T_c = 2.01(1)$ K. Taking into account the demagnetization factor derived above, the critical field value is $H_c = 342$ Oe. The full magnetization loop $M_V(H)$ measured at 1.67 K is shown in Fig. 2. The shape of the $M_V(H)$ curve—similar to other type-I superconductors, such as KBi_2 [22], $YbSb_2$ [23], and $ScGa_3$ and $LuGa_3$ [24]—together with relatively small critical field $H_c(0)$, implies that $LiPd_2Ge$ is a type-I superconductor. This is rather surprising since type-I superconductivity is unique in the intermetallic compounds and it is unusual that $LiPd_2Ge$, being a Heusler compound, would be a type-I superconductor. It is therefore

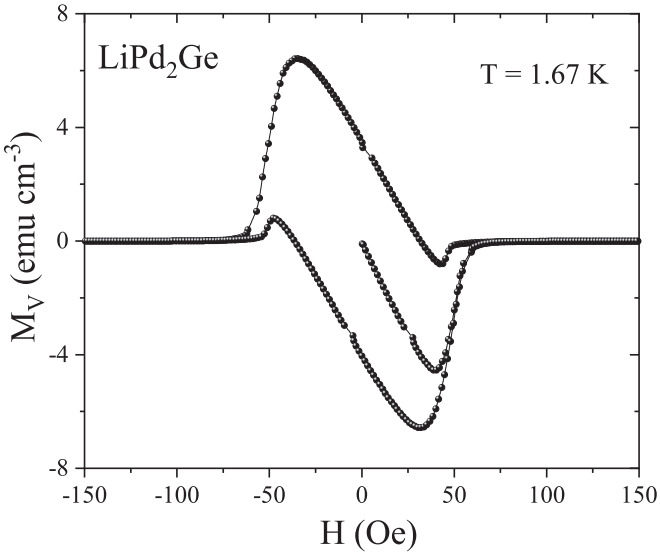

FIG. 2. Magnetization loop at $T = 1.67$ K for $LiPd_2Ge$.

important to fully characterize the superconducting state in $LiPd_2Ge$.

The main panel of Fig. 3 shows the whole temperature range of the electrical resistivity, $\rho(T)$, in zero applied magnetic field. In the normal state, the $\rho(T)$ data decrease with decreasing temperature, revealing metallicke character ($d\rho/dT > 0$). The room-temperature resistivity is approximately 194 $\mu\Omega$ cm and the residual resistivity above the critical temperature is 14 $\mu\Omega$ cm. Hence the residual resistivity ratio RRR is $\rho(300)/\rho(3) = 14$. This value is high in comparison to those reported for full-Heusler compounds, e.g., $YPd_2Sn \sim 2.5$ [8], $ZrNi_2Ga \sim 2$ [25], or $LiGa_2Rh \sim 1.2$ [11]. As shown in the inset of Fig. 3, the electrical resistivity drops to zero at $T_c = 2.04$ K, where, for resistivity data, T_c is defined by the temperature of the 50% drop of the $\rho(T)$ data in zero magnetic field. The transition temperature is slightly higher than the critical temperature obtained from the magnetic data ($T_c = 1.96$ K). When a magnetic field is applied, the superconducting transition is quickly suppressed. For a magnetic field $H = 40$ Oe, the transition width becomes wider and the superconducting temperature is 1.85 K.

The superconducting transition was further examined through specific heat measurements. Panel (a) of Fig. 4 shows the specific heat of $LiPd_2Ge$ measured from 1.81 to 300 K in zero magnetic field. At high temperatures, the experimental heat capacity $C_p(T)$ approaches the value of $3nR \approx 100\,\mathrm{J\,mol^{-1}\,K^{-1}}$ consistent with the Dulong-Petit law. Here $n = 4$ and $R = 8.31\,\mathrm{J\,mol^{-1}\,K^{-1}}$ are the number of atoms per formula unit and the ideal gas constant, respectively. The blue solid line corresponds to the whole temperature fit of a combined model: $C_p = C_{el.} + C_{\mathrm{Debye}} + C_{\mathrm{Einstein1}} + C_{\mathrm{Einstein2}}$, where $C_{el.}$ is an electronic specific heat, whereas C_{Debye} and $C_{\mathrm{Eisntein1}}$ and $C_{\mathrm{Eisntein2}}$ are the phonon specific heat contributions to C_p. Such a model, with two Einstein terms, is required to describe phonon contribution to the specific heat over a broad temperature range, because in the phonon spectrum of $LiPd_2X$ we observed two groups of separated, Einstein-like phonon modes (see below). Each consists of

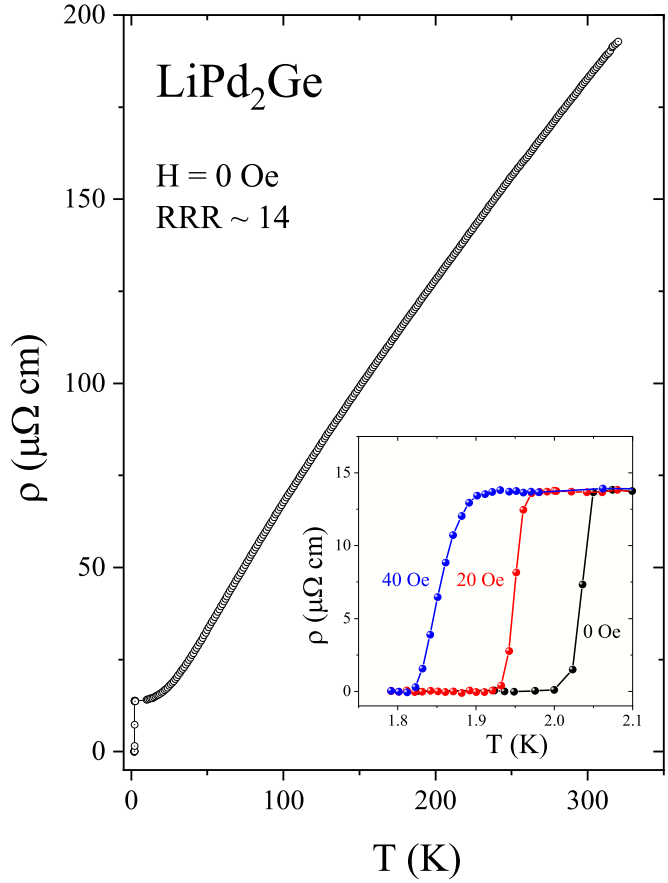

FIG. 3. The electrical resistivity of $LiPd_2Ge$ versus temperature measured in zero applied magnetic field. The inset shows the expanded plot of $\rho(T)$ in the vicinity of the superconducting transition for different values of $H = 0$, 20, and 40 Oe field.

three optic modes, gathered around characteristic ω_{E1} and ω_{E2} frequencies. Thus, the contribution to the specific heat from all such modes is equal to

$$C_{\mathrm{Einstein}}(T) = 3R\left(\frac{\Theta_E}{T}\right)^2 \exp\left(\frac{\Theta_E}{T}\right)\left[\exp\left(\frac{\Theta_E}{T}\right) - 1\right]^{-2}, \tag{2}$$

where $\hbar\omega_E = k_B\Theta_E$. As the number of atoms in the unit cell is equal to 4, from the total number of 12 phonon modes, the contribution from the remaining six modes is described in the Debye approximation, as

$$C_{\mathrm{Debye}}(T) = 2\left\{9R\left(\frac{T}{\Theta_D}\right)^3 \int_0^{\theta_D} \frac{x^4 \exp(x)}{[\exp(x) - 1]^2} dx\right\}. \tag{3}$$

The multiplier 2 assures the correct total contribution to the specific heat from the lower-frequency part of the spectrum. In this fit we fixed the Sommerfeld parameter (γ) value, obtained from the low-temperature analysis discussed below.

The blue solid line is the fitted sum of the all phonon contributions to the specific heat. The fit is excellent and the obtained parameters are $\Theta_D = 182(1)$ K, $\Theta_{E1} = 262(1)$ K, and $\Theta_{E2} = 537(1)$ K. A similar analysis was performed for the other two compounds, $LiPd_2Si$ and $LiPd_2Sn$, and the

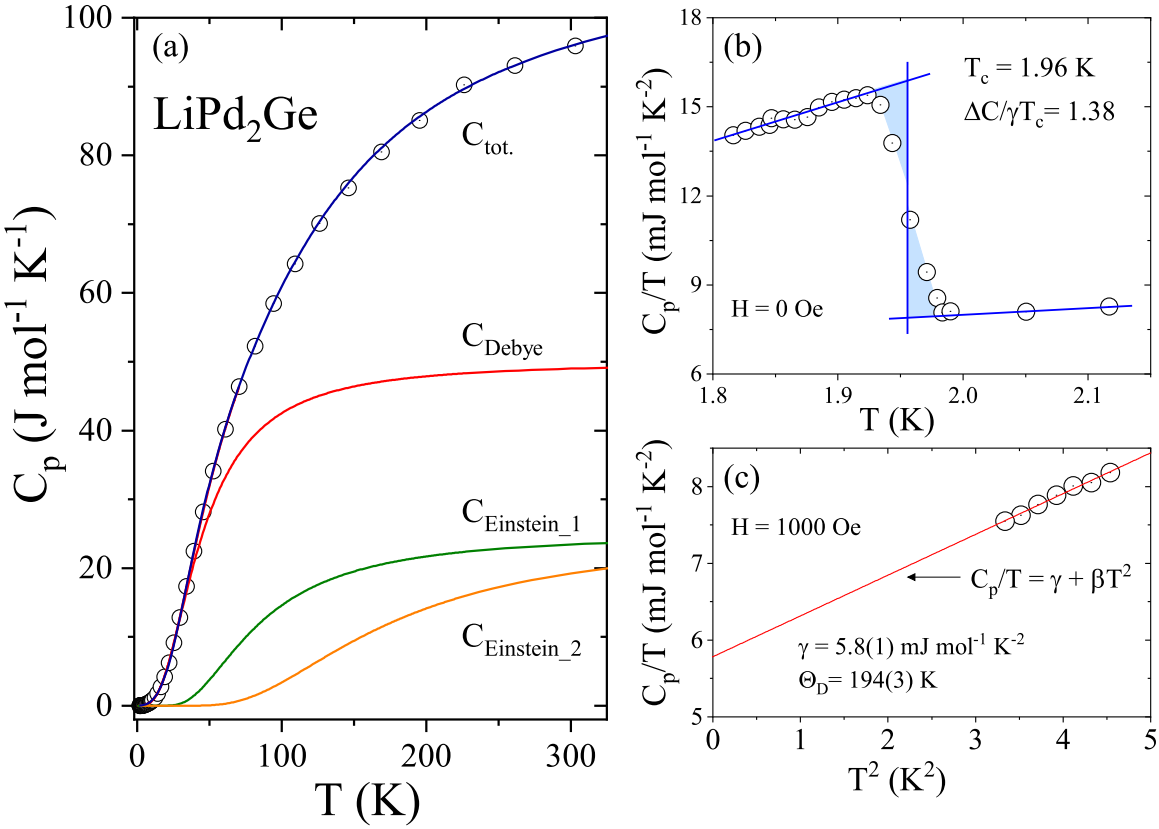

FIG. 4. Panel (a): The specific heat of $LiPd_2Ge$ versus temperature in zero magnetic field with a fit to a combined model (blue solid line): $C_p = C_{el.} + C_{\text{Debye}} + C_{\text{Einstein1}} + C_{\text{Einstein2}}$. (b) Zero-field specific heat divided by temperature (C_p/T) versus temperature. (c) C_p/T versus T^2 measured at 1000 Oe magnetic field. The red solid line represents the linear fit used to estimate the values of the electronic and phonon specific heat coefficients.

results are presented in Figs. 5 and 6. The characteristic temperatures obtained are gathered in Table II.

As shown in the expanded plot of low-temperature data collected in zero magnetic field in Fig. 4(b), a sharp jump is observed at 1.96 K, confirming the bulk nature of the superconductivity and good quality of the sample. The superconducting transition temperature ($T_c = 1.96$ K) is in good agreement with the magnetization and resistivity measurements. The specific heat jump at the critical temperature, estimated by using the equal entropy construction (blue solid

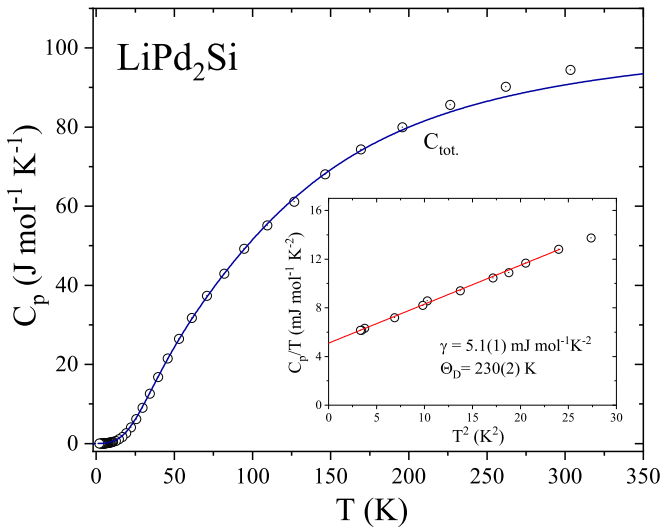

FIG. 5. Main panel: the specific heat of $LiPd_2Si$ measured from 1.8 to 300 K under zero magnetic field. Inset: C_p/T data versus T^2.

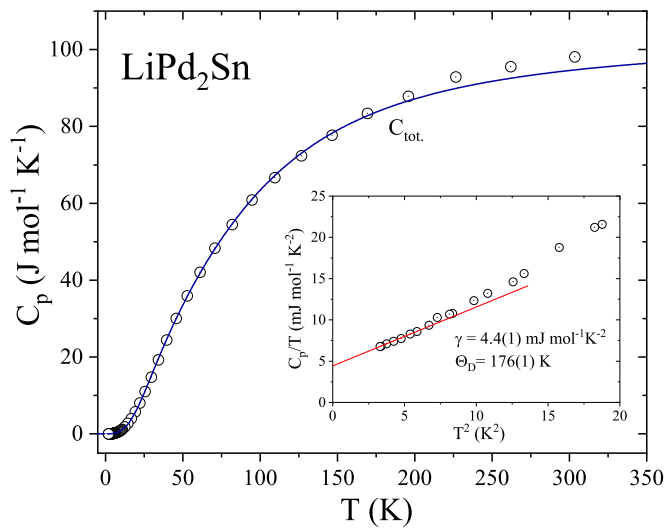

FIG. 6. Main panel: the specific heat of $LiPd_2Sn$ measured from 1.8 to 300 K under zero magnetic field. Inset: C_p/T data versus T^2.

TABLE II. Characteristic temperatures derived from a combined fit to the heat capacity. The larger differences between theoretical and experimental $\Theta_{\text{Einstein2}}$ are likely caused by small contribution of high-frequency phonons to specific heat up to 300 K and thermal expansion effects, important at higher temperatures.

$LiPd_2X$	Θ_D (K)	$\Theta_{\text{Einstein1}}$ (K)	$\Theta_{\text{Einstein2}}$ (K)
Si	211(1)/230(2)[a]	398(6)/362[b]	554(9)/604[b]
Ge	182(1)/194(3)[a]	262(1)/246[b]	537(1)/549[b]
Sn	168(1)/176(1)[a]	282(5)/240[b]	440(6)/487[b]

[a]Values estimated from a low-temperature fit.
[b]Temperatures estimated from theoretical calculations as the mean phonon frequencies around Einstein-like $F(\omega)$ peaks.

lines), is found to be about $\Delta C/T_c = 7.9\,\text{mJ mol}^{-1}\,\text{K}^{-2}$. Low-temperature $C_p(T)$ data collected under small magnetic field (up to 30 Oe) are shown in Fig. S7 in the SM [19]. The $\Delta C/T_c$ jump observed under 5 Oe measurement is slightly larger than $\Delta C/T_c$ at zero field, which might confirm type-I superconductivity proposed by field-dependent magnetization studies.

Figure 4(c) presents the heat-capacity data plotted as C_p/T versus T^2, under an applied magnetic field of $H = 1000$ Oe, which is above H_c. In the normal state the experimental data can be fitted using the formula $C_p/T = \gamma + \beta T^2$, where the first term is the electronic specific heat coefficient and the second one accounts for the lattice contribution. Fitting the data yields $\gamma = 5.8(1)\,\text{mJ mol}^{-1}\,\text{K}^{-2}$ and $\beta = 0.531(3)\,\text{mJ mol}^{-1}\,\text{K}^{-4}$. The Debye temperature can be then calculated via the relation

$$\Theta_D = \left(\frac{12\pi^4}{5\beta} nR\right)^{1/3}, \tag{4}$$

where $n = 2$ corresponds to our combined Debye + Einstein model, described above. In such a case, β corresponds to the Debye temperature of 194(3) K, in good agreement with the value obtained from the whole temperature range fit. If, instead of using the combined model, one follows the standard methodology (i.e., all the phonon modes are approximated using the Debye model) and takes $n = 4$ (number of atoms per formula unit) the resulting value of Θ_D is 244(3) K, which is comparable with those obtained for full-Heusler compounds, e.g., $LuPd_2Sn$ ($\Theta_D = 246(2)$ K [8]), $HfPd_2In$ ($\Theta_D = 243(5)$ K [8]), and $ZrPd_2In$ ($\Theta_D = 236(5)$ K [8]).

The insets of Figs. 5 and 6 present the heat-capacity data together with the fitting formula $C_p/T = \gamma + \beta T^2$. The extrapolation gives $\gamma = 5.1(1)\,\text{mJ mol}^{-1}\,\text{K}^{-2}$ for $LiPd_2Si$ and $\gamma = 4.4(1)\,\text{mJ mol}^{-1}\,\text{K}^{-2}$ for $LiPd_2Sn$. The calculated values of Θ_D (corresponding to the combined, Debye-Einstein model) are 230(2) K and 176(1) K for $LiPd_2Si$ and $LiPd_2Sn$, respectively. We do not observe any transition down to 1.81 K for either material.

Using the Sommerfeld coefficient [$\gamma = 5.8(1)$ $\text{mJ mol}^{-1}\,\text{K}^{-2}$] and the specific heat jump value at the critical temperature ($\Delta C/T_c = 7.9\,\text{mJ mol}^{-1}\,\text{K}^{-2}$), the normalized specific heat jump was then calculated. The obtained value ($\Delta C/\gamma T_c = 1.38$) is slightly lower than the value predicted by

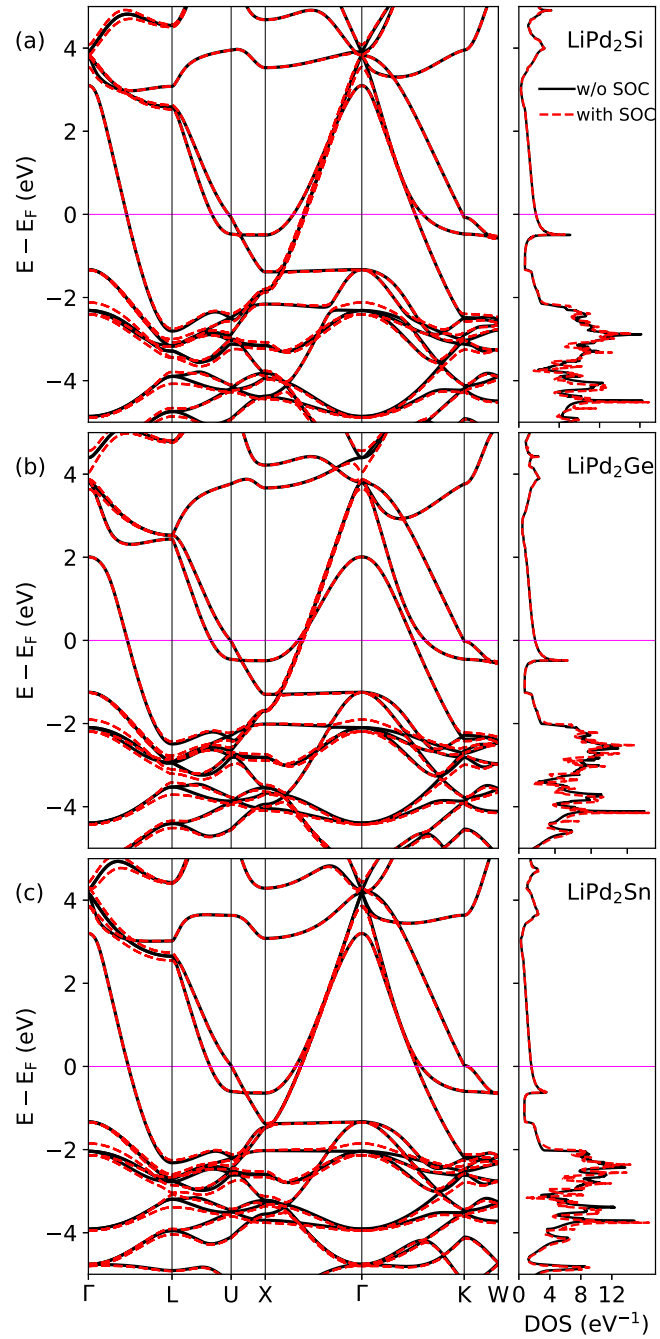

FIG. 7. Electronic structure of $LiPd_2X$ calculated without SOC (black solid lines) and including SOC (red dashed lines).

Bardeen-Cooper-Schrieffer (BCS) theory (1.43) suggesting weak-coupling superconductivity in $LiPd_2Ge$.

The electron-phonon coupling constant λ_{e-p} can be estimated from the inverted McMillan formula, which relates the Debye temperature Θ_D and the critical temperature T_c by the formula [26]

$$\lambda_{e-p} = \frac{1.04 + \mu^* \ln(\Theta_D/1.45T_c)}{(1 - 0.62\mu^*)\ln(\Theta_D/1.45T_c) - 1.04}, \tag{5}$$

where μ^* is the repulsive screened Coulomb parameter, typically taken as $\mu^* = 0.13$ for many metal systems [27–29].

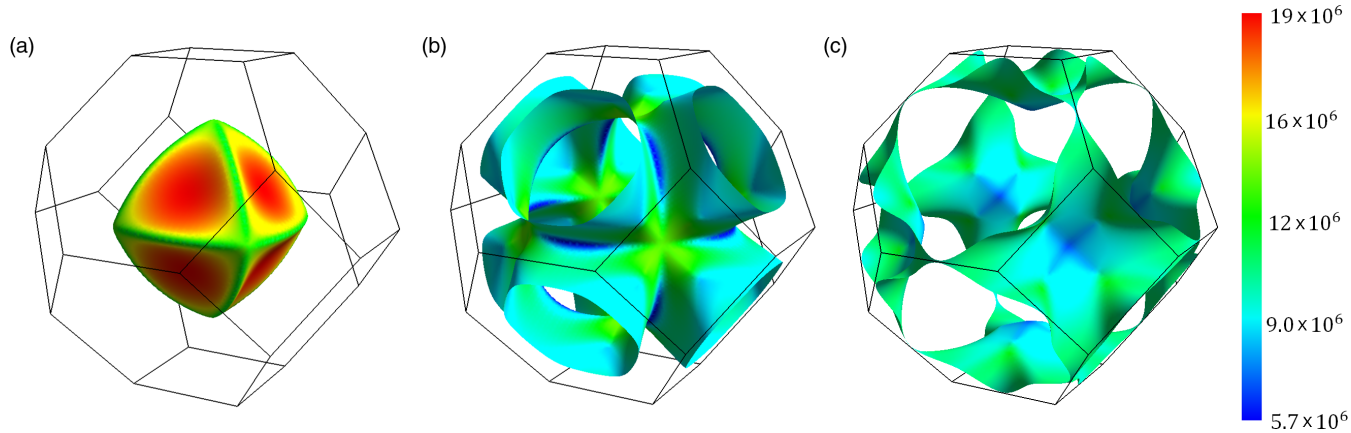

FIG. 8. Fermi surface of $LiPd_2Ge$, consisting of three sheets. Color represents the velocity of electrons (in m/s). Contribution of each sheet to the total DOS at E_F is (a) 0.25 eV^{-1}, (b) 0.90 eV^{-1}, and (c) 0.65 eV^{-1}.

Using $T_c = 1.96$ K and the Debye temperature, we obtain $\lambda_{e-p} = 0.53$ for $\Theta_D = 244$ K or $\lambda_{e-p} = 0.56$ for $\Theta_D = 194$ K, which implies that $LiPd_2Ge$ is a weak-coupling superconductor.

With the electron-phonon coupling parameter λ_{e-p} and the Sommerfeld coefficient γ known, the density of states at the Fermi energy DOS(E_F) can be calculated using the relation [30]

$$\mathrm{DOS}(E_F) = \frac{3\gamma}{\pi^2 k_B^2 (1+\lambda_{e-p})}, \tag{6}$$

where k_B is the Boltzmann constant. DOS(E_F) is estimated to be 1.6 states eV^{-1} per formula unit (f.u.).

IV. *AB INITIO* COMPUTATIONS

A. Electronic structure

Figure 7 shows the computed electronic band structure and total density of states (DOS) calculated with and without spin-orbit coupling (SOC). The effect of SOC on the electronic structure near the Fermi energy (E_F) was found to be negligible for all three compounds. However, for some upper- and lower-lying states, band splitting, band anticrossings, and degeneracy removal due to SOC can be noticed. Three electronic bands are crossing E_F, building up three Fermi surface (FS) sheets, presented in Fig. 8 for the representative example of $LiPd_2Ge$. The other $LiPd_2X$ compounds studied, which are isostructural and isoelectronic, have very similar FS.

The total DOS and partial DOS for each atom in $LiPd_2X$ are shown in Figs. 9(a)–9(c), whereas Figs. 9(d)–9(f) display the DOS projected on atomic orbitals for $LiPd_2Ge$. States near the Fermi energy are built up mainly from Pd-4d and X atom orbitals (Si-3p, Ge-4p, and Sn-5p), with the smallest contribution from Li. The Fermi level is located on a decreasing slope of a local DOS maximum, associated with Pd-4d states, and thus doping $LiPd_2X$ with holes could be a promising strategy for increasing DOS(E_F) and, potentially, T_c. Total DOS(E_F), band structure value of the Sommerfeld coefficient $\gamma_{\mathrm{band}} = \pi^2/3k_B^2\mathrm{DOS}(E_F)$, and the electron-phonon coupling constant λ_γ derived from the comparison of γ_{band} to the measured $\gamma = \gamma_{\mathrm{band}}(1+\lambda_\gamma)$ are collected in Table III. In qualitative agreement with experiment, the largest DOS(E_F) and γ_{band} is found for $LiPd_2Ge$ and the lowest for $LiPd_2Si$, which correlates with the presence of superconductivity, found above 1.68 K only in $LiPd_2Ge$. The computed renormalization parameters λ_γ are relatively small, 0.28, 0.37, and 0.16, for X = Si, Ge, and Sn, respectively. For the case of $LiPd_2Ge$, where $\lambda \approx 0.55$ was estimated experimentally, the underestimation is over 30%. This suggests that the computed DOS(E_F) value is too large, which may be related to using the ideal Heusler crystal structure in the calculations, while site-atomic disorder is usually seen in this family [7,31]. A structural distortion may also be possible due to the unstable phonon mode (see below).

Our results for $LiPd_2Ge$, as far as the shape of the DOS(E_F) curve is concerned, are similar to recently reported ones by Ayhan and Kavak Balcı [32]; however their DOS values are roughly two times smaller, with DOS(E_F) = 0.99 eV^{-1}, compared to our 1.81 eV^{-1}. As this difference by a factor of 2 occurs for the whole DOS spectrum, we suspect that the DOS in [32] is given per spin direction. However, to double-check and independently verify our computed densities, we performed calculations by using the same full-potential linearized augmented plane-wave method (FP-LAPW) and the WIEN2K package [33] as in [32]. The calculations gave almost exactly the same electronic structure that we obtained from the pseudopotential calculations in QUANTUM ESPRESSO, and confirmed the DOS(E_F) = 1.8 eV^{-1} value.

To support our claim of the type-I superconductivity in $LiPd_2Ge$ a theoretical estimation of the Ginzburg-Landau parameter $\kappa_{\mathrm{GL}} = \lambda_{\mathrm{GL}}/\xi_{\mathrm{GL}}$ has been done, where λ_{GL} and ξ_{GL} are the Ginzburg-Landau penetration depth and coherence length, respectively. First, we have to compare the BCS coherence length ξ_0 [34],

$$\xi_0 \cong 0.180\,\frac{\hbar v_F}{k_B T_c}, \tag{7}$$

with the electronic mean-free path $l_0 = v_F\tau$, to verify whether we are in the clean ($l_0 \gg \xi_0$) or dirty ($l_0 \ll \xi_0$) limit. In the above formulas, v_F is the Fermi velocity and τ is the average electronic scattering time. Values of the Fermi velocity, as shown in Fig. 8, vary between Fermi surface sheets from 5×10^6 m/s to 19×10^6 m/s, and the average $\sqrt{v_F^2} \cong 10^7$ m/s.

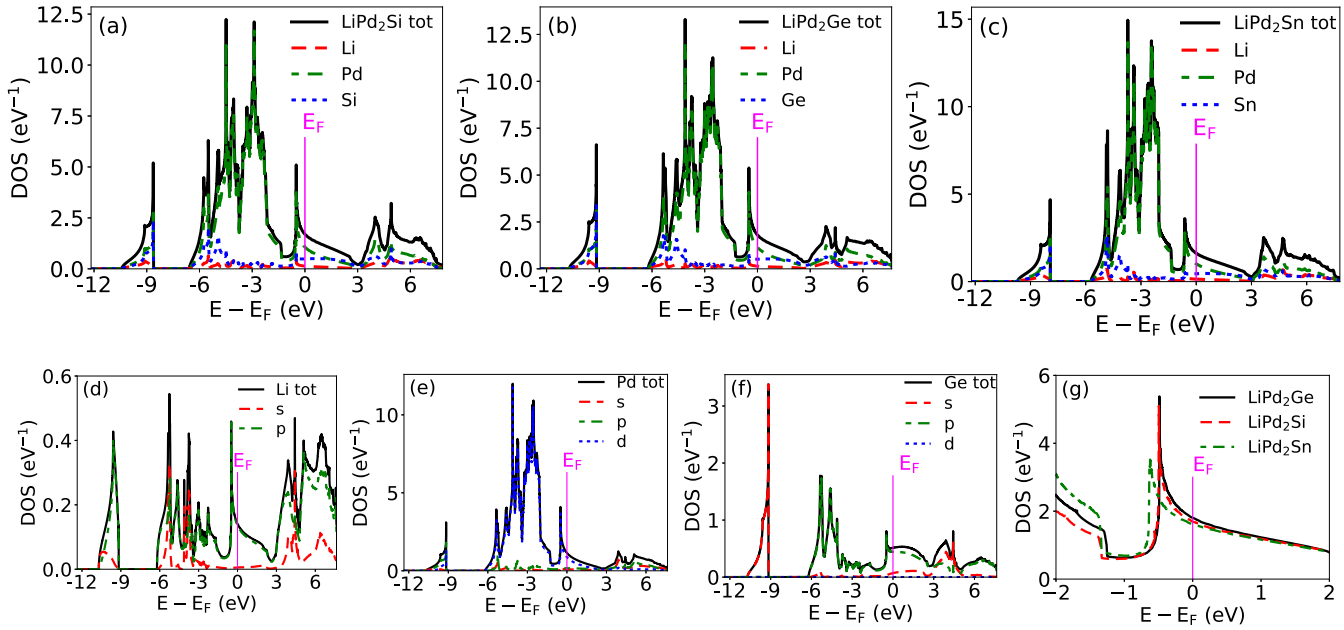

FIG. 9. The density of states (DOS) of (a) $LiPd_2Si$, (b) $LiPd_2Ge$, (c) $LiPd_2Sn$; (d–f) partial DOS of $LiPd_2Ge$; and (g) close-up of DOS near E_F for all three compounds.

This puts ξ_0 in the range 35 000–130 000 Å. To properly estimate the electronic scattering time we have calculated the electrical conductivity of $LiPd_2Ge$ from the computed band structure using the Boltzmann formalism in the constant scattering time approximation, as implemented in the BOLTZTRAP code [35]. The resulting value is $\sigma/\tau = 9.5 \times 10^{21}\,\Omega^{-1}\,\mathrm{m}^{-1}\,\mathrm{s}^{-1}$. Next, taking the experimental value of the residual resistivity, measured in Fig. 3 just above transition to the superconducting state, $\rho_0 = 13.7\,\mu\Omega\,\mathrm{cm}$, we arrive at $\tau = 7.5 \times 10^{-15}$ s. Combining τ with the average Fermi velocity we get $l_0 = 750$ Å (or l_0 in the range 400–1400 Å, while using the minimum and maximum Fermi velocity from different parts of the Fermi surface), much smaller than the BCS coherence length ξ_0, estimated above. This puts our analysis to the dirty limit, where [34]

$$\kappa_{\mathrm{GL}} \simeq 0.72\frac{\lambda_L}{l_0}. \tag{8}$$

TABLE III. Calculated density of states at Fermi energy $\mathrm{DOS}(E_F)$, Sommerfeld coefficient γ_{band}, and electron-phonon coupling constant λ_γ from the band structure compared with the experimental results. λ_{expt} is calculated using the experimental T_c and the McMillan formula.

	$LiPd_2Si$	$LiPd_2Ge$	$LiPd_2Sn$
$\mathrm{DOS}(E_F)(\mathrm{eV}^{-1})$	1.69	1.81	1.62
$\gamma_{\mathrm{band}}(\mathrm{mJ\,mol^{-1}\,K^{-2}})$	3.99	4.26	3.82
$\gamma_{\mathrm{expt}}(\mathrm{mJ\,mol^{-1}\,K^{-2}})$	5.1(1)	5.8(1)	4.4(1)
λ_{expt}	–	∼0.55	–
$\lambda_\gamma = \gamma_{\mathrm{expt}}/\gamma_{\mathrm{band}} - 1$	0.28	0.37	0.16

λ_L is the zero-temperature London penetration depth, which is calculated as

$$\lambda_L^2 = 3\,\frac{1}{\mu_0 e^2 v_F^2 \mathrm{DOS}(E_F)}, \tag{9}$$

where $\mathrm{DOS}(E_F)$ is given per unit energy and volume. Calculated separately for each FS sheet $\lambda_L \cong 30 - 60$ Å, whereas the average v_F and the total $\mathrm{DOS}(E_F)$ give $\lambda_L \cong 20$ Å. The final and conservative estimate on the Ginzburg-Landau parameter is then $0.01 < \kappa_{\mathrm{GL}} < 0.1$, being considerably smaller than the critical value of $1/\sqrt{2} \cong 0.7$. Thus, $LiPd_2Ge$ is indeed a type-I superconductor.

B. Phonons and the electron-phonon coupling

Figure 10 shows the computed phonon dispersion relations and phonon density of states $F(\omega)$ in $LiPd_2X$. In the dispersion plots, the thick blue lines represent phonon linewidths $\gamma_{\mathbf{q}\nu}$, which are a local measure of the electron-phonon coupling, discussed below. There are four atoms in the primitive cell of $LiPd_2X$, contributing to 12 phonon modes, three acoustic and nine optic. The average total and partial frequencies are collected in Table IV. The global average phonon frequency decreases with the increase of the mass of the X element, in agreement with expectations. As the partial atomic phonon DOS shows, the well-separated, Einstein-like highest-frequency optic modes are associated with Li vibrations, due to the smallest Li atomic mass ($M_{\mathrm{Li}} = 6.94$ u, $M_{\mathrm{Pd}} = 106.42$ u, $M_{\mathrm{Si}} = 28.09$ u, $M_{\mathrm{Ge}} = 72.63$ u, $M_{\mathrm{Sn}} = 118.71$ u). The average frequency of these modes also moves down when the atomic mass of the X element is changed, from ∼12.3 THz (X = Si), via 11.2 THz (X = Ge), to 10 THz (X = Sn). The second group of optic modes, also with a small dispersion, is located around 7.5 THz for X = Si and 5 THz in the two remaining cases. These modes are associated mostly with Si

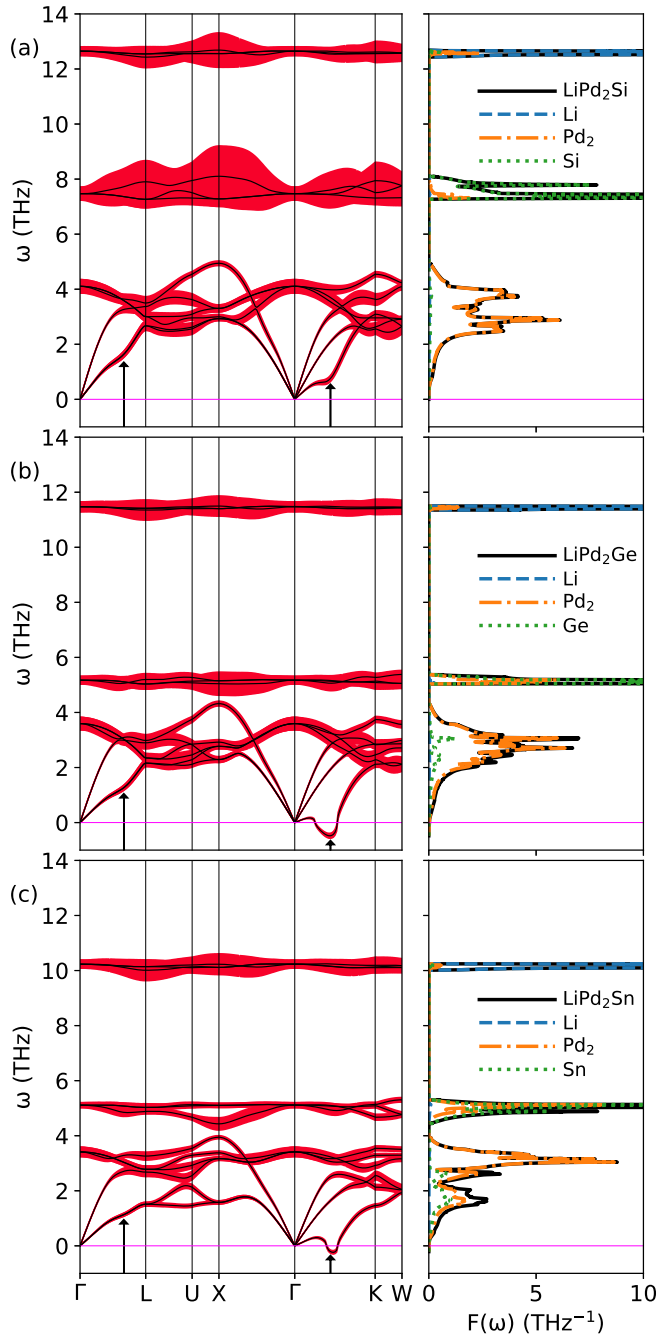

FIG. 10. Phonon dispersion relations with phonon linewidths in THz marked as thick red lines, and phonon density of states with atomic contributions. Phonon linewidths $\gamma_{\mathbf{q}\nu}$ are multiplied by 70 to improve their visibility. Arrows represent $\mathbf{q}$ vectors for which phonon anomalies occur: $\mathbf{q}_{\Gamma L} = (1/3, 1/3, 1/3)$ and $\mathbf{q}_{\Gamma K} = (1/3, 1/3, 0)$.

vibrations in $LiPd_2Si$, whereas in the two other cases they have a mixed Pd + Ge (Sn) character. A similar situation is found for the lowest part of the phonon spectrum, consisting of three acoustic and three low-frequency optic modes. For $X = Si$ it is contributed mostly by the two Pd atoms' vibrations, whereas in the two remaining compounds, a larger contribution from Ge (Sn) is found. To verify the correctness of the calculated phonon spectra, lattice specific heat was calculated, and compared to the measured one. Results are presented in the Supplemental Material [19]. The differences, seen at higher temperatures, are most likely due to anharmonic effects (thermal expansion) and likely are responsible for the differences in the experimental and theoretical Einstein mode temperatures, as shown in Table II.

TABLE IV. Calculated average phonon frequencies, electron-phonon coupling constant, critical temperature (using $\mu^* = 0.10$), and renormalized Sommerfeld coefficient. For $LiPd_2Ge$ and $LiPd_2Sn$, due to the presence of the soft mode with imaginary frequencies, for $\langle\omega_{\log}^{\alpha^2F}\rangle$ and λ_{e-p} we give a range of values, estimated based on extrapolation of the Eliashberg function, as discussed in the Supplemental Material [19]. The soft mode, however, has negligible effect on the average ω.

$LiPd_2X$	X = Si	X = Ge	X = Sn
$\langle\omega_{\text{tot}}\rangle$ (THz)	6.59	5.45	5.05
$\langle\omega_{\text{Li}}\rangle$ (THz)	12.31	11.22	10.02
$\langle\omega_{\text{Pd1}}\rangle$ (THz)	3.37	3.03	3.12
$\langle\omega_{\text{Pd2}}\rangle$ (THz)	3.37	3.03	3.12
$\langle\omega_X\rangle$ (THz)	7.29	4.51	3.96
$\langle\omega_{\log}^{\alpha^2F}\rangle$ (THz)	3.22	2.21–2.95	2.02 – 2.68
$\langle\omega_{\log}^{\alpha^2F}\rangle$ (K)	155	106–142	97 – 129
λ_{e-p} (Modes 2–12)	0.30	0.33	0.26
λ_{e-p} (Total)	0.41	0.40 – 0.52	0.32 – 0.40
T_c (K) (Calc.)	0.76	0.60 – 1.50	0.11 – 0.41
T_c (K) (Expt.)	–	1.96	–

The most intriguing features of the computed phonon spectra are phonon anomalies observed in the acoustic modes in each of the studied compounds. A soft mode is detected for the transverse acoustic mode in the Γ-K direction, with a minimum frequency near $\mathbf{q}_{\Gamma K} = (1/3, 1/3, 0)$, denoted by the arrow in Fig. 10. In the case of $LiPd_2Si$, frequency is significantly lowered, whereas for X = Ge and Sn frequencies become imaginary (plotted as negative in Fig. 10). We label this mode as a "soft" one in the remaining part of the paper, although in the X = Si case frequency is positive. In addition, in the Γ-L direction at $\mathbf{q}_{\Gamma L} = (1/3, 1/3, 1/3)$ a weaker softening resembling, e.g., the Kohn anomaly in Pb [36] is seen. To rule out the possibility that the detected instability is a result of the choice of pseudopotential or insufficient q-point sampling (equivalent to insufficient number of neighboring atoms considered in calculations of interatomic force constants), we have performed test calculations for $LiPd_2Ge$ with three different sets of pseudopotentials, and for all compounds, using three sizes of q-point grid: 4^3, 6^3, 8^3. The results are summarized in the Supplemental Material [19]. As far as the choice of pseudopotential is concerned, only very small differences in frequencies of higher-frequency modes were noticed (due to the slightly smaller lattice parameter), leaving the soft mode unchanged. For the q-point grid test, the 4^3 mesh was found to be too coarse, and starting from the 6^3 mesh, convergent results were obtained. Additionally, for $LiPd_2Ge$ inclusion of spin-orbit coupling had no effect on either the soft mode or on the other phonon branches; these are checked in calculations for two selected q-points; see Fig. S2 [19].

Phonon anomalies are frequently observed in Heusler compounds. Among the possible reasons for such behavior we may distinguish Kohn anomalies due to Fermi surface nesting, martensitic instabilities towards modulated structures, or the formation of charge density waves [37–44]. In particular, a soft mode in the Γ-*K* direction at a similar wave vector $\mathbf{q}_{\Gamma K}$ was observed in several magnetic and nonmagnetic materials, including the widely studied magnetic shape-memory alloy Ni_2MnGa. Martynov and Kokorin [38], in x-ray diffraction studies, showed the presence of many thermally and stress-induced martensitic phase transitions and structure modulations. Zheludev *et al.* found soft modes in Ni_2MnGa in inelastic neutron scattering [39] and concluded that the phonon anomalies are probably caused by electron-phonon interactions. Zayak *et al.* [37] studied with *ab initio* calculations anomalous vibrations in magnetic and nonmagnetic Heusler compounds. They observed that compounds with anomalies in their phonon structure also had low-lying optical modes at Γ. Modes of the same symmetry repel each other, so they argued that these optical modes pushed acoustic modes down which softened them. Low-lying optical modes could be caused by additional covalent bonding in dominantly metallic Ni_2MnGa. Both magnetic and nonmagnetic compounds were found to have soft modes, and therefore magnetic order is not a condition for phonon anomalies in those compounds. They also pointed out that valence electron number per atom is an important quantity, because it could be used to classify stable and unstable ferromagnetic structures, where stable compounds had this ratio below 7.4. In the case of $LiPd_2X$ it is equal to 6.25, and thus it does not follow this rule. In our work we have not found any signs of phase transition in $LiPd_2X$ in the heat-capacity or resistivity measurements. It is worth noting, that in recent work on related $LiGa_2Rh$ [45], acoustic mode softening, similar to our case of $LiPd_2Si$, was detected, without imaginary frequencies.

As far as the "atomic" character of the soft mode near the minimum frequency is concerned, in all compounds it has generally equal contributions from Pd1, Pd2, and *X* atoms (even for $X = Si$, where contribution of Si to remaining parts of the low-frequency spectrum is small). Phonon displacement patterns for the unstable mode at $\mathbf{q}_{\Gamma K} = (1/3, 1/3, 0)$ for $LiPd_2Ge$ are visualized in Fig. 11. Pd and Ge vibrate in phase with each other and out of phase with small-amplitude Li vibrations. That could indicate a tendency towards an uniform distortion of the cubic structure. As the origin of soft modes is a broad and interesting issue requiring deeper studies we leave it for future works, here pointing only to their possible connection to superconductivity.

To describe superconductivity in $LiPd_2X$ we assumed an electron-phonon pairing mechanism with the Migdal-Eliashberg theory. The electron-phonon interaction matrix elements, computed using perturbation theory in QE, allow us to calculate the phonon linewidths $\gamma_{\mathbf{q}\nu}$ (see, e.g., [46,47]), already presented in Fig. 10. Besides an enhancement of $\gamma_{\mathbf{q}\nu}$ for Si vibrations in Fig. 10(a), we do not see any specific mode or direction dependence of linewidths. Weighted by an inverse square frequency, $\gamma_{\mathbf{q}\nu}$ measures the local contribution of a phonon to the global electron-phonon coupling parameter

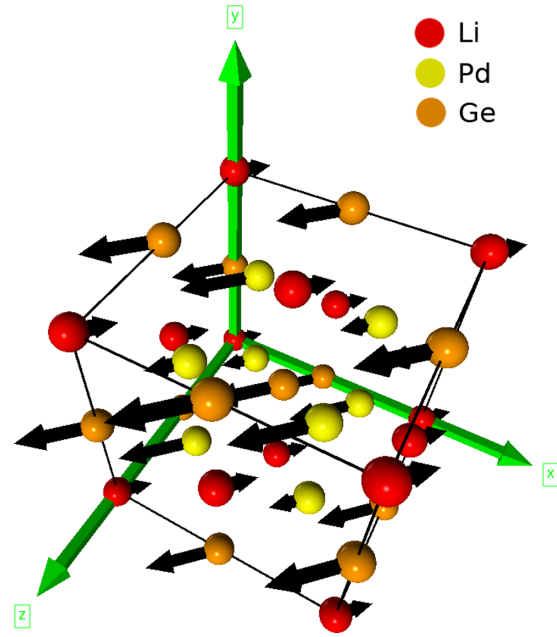

FIG. 11. Visualization of atomic vibrations with $\mathbf{q} = (1/3, 1/3, 0)$, for the first transverse acoustic mode of $LiPd_2Ge$. Red balls represent Li, orange balls in the middle of the edges and one in the middle of the cell represent Ge, and yellow balls inside the cube represent Pd. Pd and Ge vibrate in phase with each other and out of phase with Li.

λ_{e-p}:

$$\lambda_{e-p} = \sum_{\boldsymbol{q},\nu} \frac{\gamma_{\boldsymbol{q}\nu}}{\pi \hbar N(E_F)\omega^2_{\boldsymbol{q},\nu}}, \tag{10}$$

where $N(E_F)$ is the total DOS at the Fermi level. By summing over all phonon modes ν and wave vectors $\mathbf{q}$, the Eliashberg electron-phonon interaction function $\alpha^2F(\omega)$ is calculated:

$$\alpha^2F(\omega) = \frac{1}{2\pi N(E_F)} \sum_{\boldsymbol{q}\nu} \delta(\omega - \omega_{\boldsymbol{q}\nu}) \frac{\gamma_{\boldsymbol{q}\nu}}{\hbar\omega_{\boldsymbol{q}\nu}}, \tag{11}$$

which alternatively allows us to calculate λ_{e-p}:

$$\lambda_{e-p} = 2\int_0^{\omega_{\max}} \frac{\alpha^2F(\omega)}{\omega} d\omega. \tag{12}$$

The obtained $\alpha^2F(\omega)$ are plotted in Fig. 12, and, similar to $F(\omega)$, the Eliashberg functions have a three-peak structure. The phonon DOS is also plotted in the background in Fig. 12 after renormalization to the same value as the area under $\alpha^2F(\omega)$. This allows us to analyze for which frequency range Eliashberg function is enhanced. Some enhancement is seen for $LiPd_2Si$ [Fig. 12(a)] around 7.5 THz, due to large phonon linewidths, seen in Fig. 10(a). However, this effect is not very strong due to relatively high frequency of silicon vibrations, as $\alpha^2F(\omega) \propto \frac{\gamma_{q\nu}}{\omega_{q\nu}}$. On the other hand, in the low-frequency range we see a dominating contribution from the first "soft" mode, plotted using a dashed line in Fig. 12, which results both from the low frequency of vibrations and increased phonon linewidths at $\mathbf{q}_{\Gamma K}$. The increased $\gamma_{\mathbf{q}\nu}$ are especially

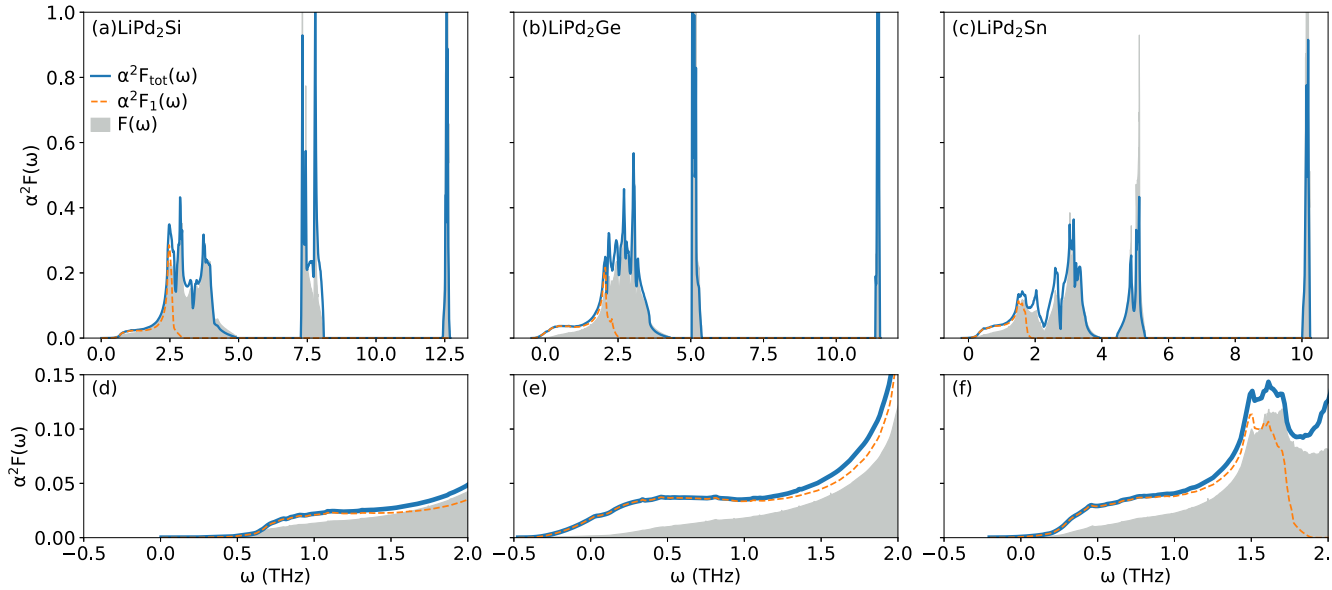

FIG. 12. Eliashberg functions for $LiPd_2X$. Orange dashed lines denote Eliashberg functions only for the first acoustic mode, whereas blue lines denote total function, summed over all 12 modes. Panels in the second row show details near zero frequency.

seen in $LiPd_2Ge$, and thus the enhancement of the Eliashberg function over the $F(\omega)$ is especially seen for this compound. Thus, superconductivity and strong soft-mode behavior are correlated in $LiPd_2X$, as the strongest electron-phonon coupling and superconductivity above 1.68 K are found for $X = Ge$.

Due to the presence of imaginary frequencies, T_c and λ_{e-p} cannot be calculated accurately for $LiPd_2Ge$ and $LiPd_2Sn$. Even though the contribution of the imaginary part of the spectrum, calculated as an area under the phonon DOS curve, is only 0.05% in $LiPd_2Ge$ and 0.005% in $LiPd_2Sn$, the enhanced values of $\alpha^2F(\omega)$ for the soft mode and $\lambda_{e-p} \propto \frac{\gamma_{qv}}{\omega_{qv}{}^2}$ dependencies make the contribution of the low-frequency phonon modes to λ_{e-p} especially important. To be able to quantify the electron-phonon coupling strength and analyze its magnitude along the series of compounds, at first we calculated the contribution to λ_{e-p} from all the modes except the first, "soft" one. The values are shown in Table IV as λ_{e-p} (modes 2–12) and increase from 0.26 ($X = Sn$), via 0.30 ($X = Si$), to 0.33 ($X = Ge$). The contribution from the first mode in $LiPd_2Si$ is equal to 0.11, resulting in total $\lambda_{e-p} = 0.41$. The direct calculation of $\lambda_{e-p(1)}$ associated with the first mode in $X = Ge$ and Sn is impossible due to the divergent behavior of $\alpha^2F(\omega)/\omega$ near $\omega = 0$. To overcome this difficulty and estimate first mode contributions, we have extrapolated $\alpha^2F(\omega)$ in two ways to set approximate upper and lower bounds for the computed $\lambda_{e-p(1)}$; the details are described in the Supplemental Material [19]. The resulting values are in the range of $\lambda_{e-p(1)} = 0.07 - 0.19$ ($X = Ge$) and $\lambda_{e-p(1)} = 0.06 - 0.14$ ($X = Sn$), giving the ranges of calculated total $\lambda_{e-p} = 0.40 - 0.52$ for $LiPd_2Ge$ and $\lambda_{e-p} = 0.32 - 0.40$ for $LiPd_2Sn$. Within the same method, the logarithmic average frequency $\langle\omega_{\log}^{\alpha^2F}\rangle$ was calculated (see Table S-II and the Supplemental Material [19]), as it is also defined based on the Eliashberg function.

The critical temperature T_c may now be approximately computed using the Allen-Dynes [48] equation:

$$T_c = \frac{\langle\omega_{\log}^{\alpha^2F}\rangle}{1.20}\exp\left[\frac{-1.04(1+\lambda_{e-p})}{\lambda_{e-p} - \mu^*(1+0.62\lambda_{e-p})}\right], \qquad (13)$$

where $\mu^* = 0.10$, as is the case when the Allen-Dynes formula is used [48].

The results are presented in Table IV. For all compounds, the theoretical λ_{e-p} computed from the Eliashberg functions are larger than the λ_γ extracted from the electronic specific heat (see Table III). For $LiPd_2Ge$, however, it is closer to the $\lambda_{\text{expt}} \approx 0.55$ estimated from the experimental T_c. The computed value of T_c, being in the range between 0.60 and 1.50 K, is visibly lower than experimental $T_c = 1.96$ K. Note that the upper value of $\langle\omega_{\log}^{\alpha^2F}\rangle = 142$ K for T_c calculations should be used in combination with the lower estimation of $\lambda_{e-p} = 0.4$, and vice versa.

For the two other studied Heuslers, where no superconductivity above 1.68 K was experimentally found, the computed T_c is lower, 0.76 K for $X = Si$ and 0.26 ± 0.15 K for $X = Sn$. Taking into account the inaccuracy of the electron-phonon coupling calculations due to the presence of soft modes, the qualitative agreement between theory and experiment is considered satisfactory. Calculations confirm that $LiPd_2Ge$ is a weakly coupled electron-phonon superconductor, whereas $LiPd_2Si$ and $LiPd_2Sn$ are expected to have T_c below 1 K.

V. SUMMARY

We have optimized a solid-state reaction method to obtain polycrystalline $LiPd_2X$, where $X = Si$, Ge, and Sn. LeBail analysis of the powder x-ray diffraction patterns confirm that all three compounds belong to the Heusler-type family. We have not seen reports of $LiPd_2Si$. The estimated lattice parameters for $LiPd_2Ge$ and $LiPd_2Sn$ are in good agreement with previous reports. Superconductivity was observed for

$LiPd_2Ge$ with $T_c = 1.96$ K. $LiPd_2Ge$ is another example of a superconducting material in the Pd-based Heusler-type family. Interestingly it is a type-I superconductor, unique in this system, and it has the total valence electron number $N_{el.} = 25$. Theoretical calculations suggest that the two other compounds studied should also reveal superconducting behavior but with $T_c = 0.76$ and 0.25 K for $LiPd_2Si$ and $LiPd_2Sn$, respectively.

Detailed studies of the superconducting properties show that $LiPd_2Ge$ is a BCS weakly coupled superconductor with a heat-capacity anomaly $\Delta C/\gamma T_c = 1.38$ and an electron-phonon coupling constant $\lambda_{e-p} \sim 0.55$. Type-I superconductivity is rather rare in intermetallic compounds and $LiPd_2Ge$ is unusual as a Heusler compound that is a type-I superconductor.

Detailed theoretical calculations show the presence of soft modes which likely enhance electron-phonon coupling and can be responsible for the enhanced superconductivity for $LiPd_2Ge$. Studies of the soft modes will be continued.

ACKNOWLEDGMENTS

Work at GUT was supported by the National Science Centre (Poland), Grant No. 2017/27/B/ST5/03044. Work at AGH-UST was supported by the National Science Centre (Poland), Project No. 2017/26/E/ST3/00119. The synthetic work at Princeton was supported by the US Department of Energy, Division of Basic Energy Sciences, Grant No. DE-FG02-98ER45706. T.K. would like to thank Damian Brzozowski for his assistance in preparation of $LiPd_2Sn$.

[1] F. Heusler, W. Starck, and E. Haupt, Verh. Dtsch. Phys. Ges. **5**, 220 (1903).
[2] T. Gruner, D. Jang, Z. Huesges, R. Cardoso-Gil, G. H. Fecher, M. M. Koza, O. Stockert, A. P. Mackenzie, M. Brando, and C. Geibel, Nat. Phys. **13**, 967 (2017).
[3] S. Chadov, X. Qi, J. Kübler, G. H. Fecher, C. Felser, and S. C. Zhang, Nat Mater. **9**, 541 (2010).
[4] B. Nowak, O. Pavlosiuk, and D. Kaczorowski, J. Phys. Chem. C **119**, 2770 (2015).
[5] O. Pavlosiuk, D. Kaczorowski, X. Fabreges, A. Gukasov, and P. Wiśniewski, Sci Rep. **6**, 18797 (2016).
[6] Y. Pan, A. M. Nikitin, T. V. Bay, Y. K. Huang, C. Paulsen, B. H. Yan, and A. de Visser, EPL **104**, 27001 (2013).
[7] T. Graf, C. Felser, and S. S. P. Parkin, Prog. Solid State Chem. **39**, 1 (2011).
[8] T. Klimczuk, C. H. Wang, K. Gofryk, F. Ronning, J. Winterlik, G. H. Fecher, J.-C. Griveau, E. Colineau, C. Felser, J. D. Thompson, D. J. Safarik, and R. J. Cava, Phys. Rev. B **85**, 174505 (2012).
[9] B. T. Matthias, Phys Rev. **97**, 74 (1955).
[10] S. V. Vonsovskii, I. A. Iziumov, and È. Z. Kurmaev, *Superconductivity of Transition Metals: Their Alloys and Compounds* (Springer-Verlag, Berlin, 1982).
[11] E. M. Carnicom, W. Xie, Z. Yang, K. Górnicka, T. Kong, T. Klimczuk, and R. J. Cava, Chem Mater. **31**, 2164 (2019).
[12] B. T. Matthias, Phys Rev. **92**, 874 (1953).
[13] P. Giannozzi, S. Baroni, N. Bonini, M. Calandra, R. Car, C. Cavazzoni, D. Ceresoli, G. L. Chiarotti, M. Cococcioni, I. Dabo, A. Dal Corso, S. de Gironcoli, S. Fabris, G. Fratesi, R. Gebauer, U. Gerstmann, C. Gougoussis, A. Kokalj, M. Lazzeri, L. Martin-Samos *et al.*, J Phys.: Condens. Matter **21**, 395502 (2009).
[14] P. Giannozzi, O. Andreussi, T. Brumme, O. Bunau, M. Buongiorno Nardelli, M. Calandra, R. Car, C. Cavazzoni, D. Ceresoli, M. Cococcioni, N. Colonna, I. Carnimeo, A. Dal Corso, S. de Gironcoli, P. Delugas, R. A. DiStasio, A. Ferretti, A. Floris, G. Fratesi, G. Fugallo *et al.*, J Phys.: Condens. Matter **29**, 465901 (2017).
[15] Pseudopotentials downloaded from https://www.quantum-espresso.org/pseudopotentials: Li.pbe-s-kjpaw_psl.1.0.0.UPF; Pd.pbe-n-kjpaw_psl.1.0.0.UPF; Pd.rel-pbe-n-kjpaw_psl.1.0.0.UPF; Si.pbe-n-kjpaw_psl.1.0.0.UPF; Si.rel-pbe-n-kjpaw_psl.1.0.0.UPF; Ge.pbe-dn-kjpaw_psl.1.0.0.UPF; Ge.rel-pbe-dn-kjpaw_psl.1.0.0.UPF; Sn.pbe-dn-kjpaw_psl.1.0.0.UPF; Sn.rel-pbe-dn-kjpaw_psl.1.0.0.UPF.
[16] A. Dal Corso, Comput Mater. Sci. **95**, 337 (2014).
[17] J. P. Perdew, K. Burke, and M. Ernzerhof, Phys. Rev. Lett. **77**, 3865 (1996).
[18] S. Baroni, S. de Gironcoli, A. Dal Corso, and P. Giannozzi, Rev. Mod. Phys. **73**, 515 (2001).
[19] See Supplemental Material at http://link.aps.org/supplemental/10.1103/PhysRevB.102.024507 for more information.
[20] C.-J. Kistrup and H.-U. Schuster, Z. Anorg Allg. Chem. **410**, 113 (1974).
[21] T. Klimczuk and R. J. Cava, Phys. Rev. B **70**, 212514 (2004).
[22] S. Sun, K. Liu, and H. Lei, J. Phys.: Condens. Matter **28**, 085701 (2016).
[23] L. L. Zhao, S. Lausberg, H. Kim, M. A. Tanatar, M. Brando, R. Prozorov, and E. Morosan, Phys. Rev. B **85**, 214526 (2012).
[24] E. Svanidze and E. Morosan, Phys. Rev. B **85**, 174514 (2012).
[25] J. Winterlik, G. H. Fecher, C. Felser, M. Jourdan, K. Grube, F. Hardy, H. von Löhneysen, K. L. Holman, and R. J. Cava, Phys. Rev. B **78**, 184506 (2008).
[26] W. L. McMillan, Phys. Rev. **167**, 331 (1968).
[27] K. Górnicka, E. M. Carnicom, S. Gołąb, M. Łapiński, B. Wiendlocha, W. Xie, D. Kaczorowski, R. J. Cava, and T. Klimczuk, Supercond. Sci. Technol. **32**, 025008 (2019).
[28] K. Górnicka, R. J. Cava, and T. Klimczuk, J. Alloys Compd. **793**, 393 (2019).
[29] E. M. Carnicom, W. Xie, T. Klimczuk, J. Lin, K. Górnicka, Z. Sobczak, N. P. Ong, and R. J. Cava, Sci. Adv. **4**, eaar7969 (2018).
[30] C. Kittel, *Solid State Physics*, 4th ed. (Wiley, New York, 1966).
[31] H. C. Kandpal, V. Ksenofontov, M. Wojcik, R. Seshadri, and C. Felser, J. Phys. D: Appl. Phys. **40**, 1587 (2007).
[32] S. Ayhan and G. Kavak Balcı, Mater Res. Express **6**, 0865e9 (2019).
[33] P. Blaha, K. Schwarz, G. K. H. Madsen, D. Kvasnicka, and J. Luitz, *WIEN2K, An Augmented Plane Wave + Local Orbitals Program for Calculating Crystal Properties* (Technische Universitat Wien, Vienna, 2001).
[34] H. Bartolf, *Fluctuation Mechanisms in Superconductors* (Springer Fachmedien, Wiesebaden, Germany, 2016).

[35] G. K. H. Madsen and D. J. Singh, Comput. Phys. Commun. **175**, 67 (2006).
[36] P. Aynajian, T. Keller, L. Boeri, S. M. Shapiro, K. Habicht, and B. Keimer, Science **319**, 1509 (2008).
[37] A. T. Zayak, P. Entel, K. M. Rabe, W. A. Adeagbo, and M. Acet, Phys. Rev. B **72**, 054113 (2005).
[38] V. V. Martynov and V. V. Kokorin, J. Phys. III **2**, 739 (1992).
[39] A. Zheludev, S. M. Shapiro, P. Wochner, and L. E. Tanner, Phys. Rev. B **54**, 15045 (1996).
[40] S. Ağduk and G. Gökoğlu, J. Alloys Compd. **511**, 9 (2012).
[41] H. Kim, B. I. Min, and K. Kim, Phys. Rev. B **98**, 144305 (2018).
[42] T. Büsgen, J. Feydt, R. Hassdorf, S. Thienhaus, M. Moske, M. Boese, A. Zayak, and P. Entel, Phys. Rev. B **70**, 014111 (2004).
[43] X. Moya, L. Mañosa, A. Planes, T. Krenke, M. Acet, V. O. Garlea, T. A. Lograsso, D. L. Schlagel, and J. L. Zarestky, Phys. Rev. B **73**, 064303 (2006).
[44] S. Paul, B. Sanyal, and S. Ghosh, J. Phys.: Condens. Matter **27**, 035401 (2015).
[45] H. Y. Uzunok, E. Karaca, S. Bağcı, and H. M. Tütüncü, Solid State Commun. **311**, 113859 (2020).
[46] R. Heid, K.-P. Bohnen, I. Y. Sklyadneva, and E. V. Chulkov, Phys. Rev. B **81**, 174527 (2010).
[47] S. Gołąb and B. Wiendlocha, Phys. Rev. B **99**, 104520 (2019).
[48] P. B. Allen and R. C. Dynes, Phys. Rev. B **12**, 905 (1975).